

Optimal Dark Current Reduction in Quantum Well 9 μm GaAs/AlGaAs Infrared Photodetectors with Improved Detectivity

¹Shahram Mohammad Nejad, ²Saeed Olyaei and ¹Maryam Pourmahyabadi
¹Optoelectronic and Laser Laboratory,
Iran University of Science and Technology, Narmak, 16846, Tehran, Iran
²Department of Electrical Engineering,
Shahid Rajaei Teacher Training University, Lavizan, 16788, Tehran, Iran

Abstract: In this research, an optimization approach is presented to decrease the dark current in GaAs/AlGaAs QWIPs. The dark current noise is reduced by increasing Al density in barriers, decreasing detector dimensions and increasing the periodic length of the structure. In addition, increasing the number of periods can reduce both the dark current and responsivity. Therefore, devices can be optimally designed through judicious choice of these parameters. An optimal photodetector structure is designed and simulated to achieve low dark current (11nA) and detectivity of $1.4 \times 10^{12} \text{cm}(\text{Hz})^{1/2}/\text{W}$ which is an order of magnitude greater than the present values.

Key words: Quantum Well Infrared Photodetector, dark current reduction, improved detectivity

INTRODUCTION

With the increasing demand for new optical application of quantum well infrared photodetectors (QWIPs) at a wide variety of wavelength from mid to far infrared, the need for low noise structure has become greater than ever. The absorption of long wavelength light in QW is due to transition from a quasi bound state to the continuum in a narrow well or intersub-band transition in a wide well. Also, QWIPs exhibit very fast operation as demonstrated in recent experiments. Their intrinsic high speed is considered as one of the advantages of the QWIPs over standard detectors made of narrow-gap semiconductors.

In the meantime, the dark current determines the signal to noise ratio of QWIPs and therefore, minimizing it, is of utmost important design criterion for their construction. By reducing QWIP dark current, photodetector can respond to weaker optical signal. The three major contributors to the dark current are: sequential tunneling, field induced emission and thermionic emission^[1-4].

The QWIP under consideration comprises a QW structure sandwiched between the emitter and collector barriers (the extreme barriers of the QW structure) with contact layers heavily doped by donors. The QW structure includes heavily-doped narrow-gap wells separated by thick undoped wide-gap barriers. The conduction band edge profile of the QWIP is shown in

Fig. 1^[5]. It is assumed that the barrier thickness L_b far exceeds the thickness of the wells L_w . The thickness and the depth of the wells are adopted in such a way that the well contains only one bound level and the first excited level corresponds to the top of the barriers between the wells. Thus the electron excitation energy is defined by the location of the bound level with respect to the barrier top.

In this research the contributors to the dark current and the methods applied to the problem of dark current reduction are discussed. Then the QWIP characteristics such as responsivity, gain and detectivity are expressed. Also, we demonstrated an optimization approach to achieve both low dark current and acceptable responsivity by judicious choice of the parameters. The photodetector in question is designed and then, the results of numerical analysis and simulation are presented.

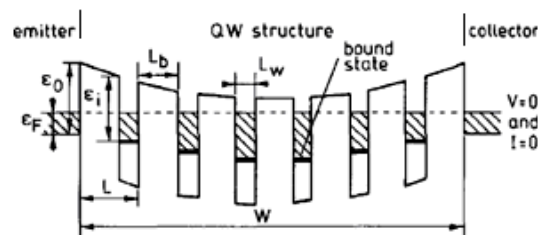


Fig. 1: Schematic view of the conduction band edge profiles for the QWIP^[5]

Corresponding Author: Saeed Olyaei, Department of Electrical Engineering, Shahid Rajaei Teacher Training University (SRTTU), Lavizan, 16788, Tehran, Iran Tel/Fax: +98 21 22970006

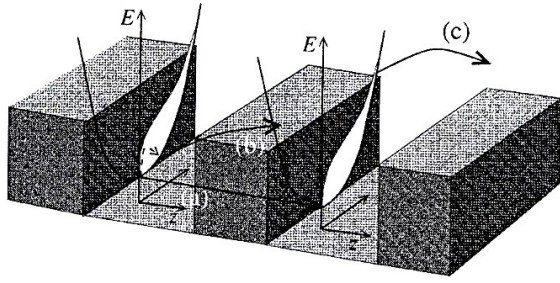


Fig. 2: Three possible mechanisms contributing to the dark current (a) Sequential tunneling, (b) Field induced emission and (c) Thermionic emission

DARK CURRENT REDUCTION

In this section, we cover the contributors to the dark current and then, the methods applied to the problem of dark current reduction are expressed in details.

The first contributor, sequential tunneling is purely electron scattering from states localized in one QW to the next (Fig. 2a). This scattering actually has to be mediated by a third party such as a phonon or another electron. This process doesn't depend on temperature. At very low temperatures (below 40°K) and sensitivity peak at 50 μm, sequential tunneling is the main factor of dark current generation.

The second, field induced emission (Fig. 2b) is again scattering mediated by either a phonon or another charge carrier, but this time, it is from upper states of the sub-band distribution. Although this reduces the “activation energy,” the number of carriers at these energies is smaller, making this process less likely to occur.

The final contribution to the dark current is due to thermionic emission (Fig. 2c). It is simply thermal excitation of the carriers directly out of the top of the QW into the continuum states above the semiconductor barriers where, they are free to move. Hence, under the influence of the applied bias, constitute a current flow. It is the main factor at high temperatures (over 45°K) and sensitivity peak at 50μm.

Reducing sequential tunneling with increased barrier width: The contribution of sequential tunneling to the dark current (based upon carrier scattering approach) can be reduced simply by increasing the width of the barrier separating adjacent wells^[6-7]. The current density is given by $J = env$, where e is the electronic charge and v is the velocity of the carriers. In the model, the electrons scatter a distance equal to the period of MQW (l_w+l_b) in the time τ given by the scattering rate as:

Table 1: Electron_Lo phonon and electron_electron scattering rates

$\lambda(\mu\text{m})$	$\Lambda(\text{\AA})$	
	$(1/\tau_{LO})$	$(1/\tau_{ee})$
7.0	8.1	7.1
7.4	8.3	7.3
7.7	8.6	7.6
8.7	9.0	7.9
9.7	9.5	8.4
11.3	10.1	9.1
14.0	11.0	10.6
19.3	12.0	14.1
32.0	17.9	27.0

$$\frac{1}{\tau} = \frac{1}{\tau_{LO}} + \frac{1}{\tau_{ee}} \quad (1)$$

Therefore, the velocity is given by $v = (l_w + l_b) / \tau$. The higher electron_Lo ($1/\tau_{LO}$) or electron_electron ($1/\tau_{ee}$) scattering rate, the larger contribution of this mechanism to the dark current. As a result, the contribution of electron_Lo phonon and electron_electron scattering to the sequential tunneling component of the dark current increases with increasing detection wavelength. The (largely) monotonic and uniform nature of the series of curves for different barrier widths suggests for any given wavelength λ , an empirical relationship of the form:

$$(1/\tau) = \alpha e^{-l_b/\Lambda} \quad (2)$$

for both electron_Lo phonon and electron_electron scattering, where α is the absorption coefficient and Λ is a constant. Analysis proves that this is correct with the constants given in Table 1.

Examination of the data in Table 1 shows that as the detection wavelength increases from mid to far infrared values, the barrier required to reduce the sequential tunneling component of the dark current also increases. This is due to the reduced well thickness pushing the electron states toward the top of the barrier, allowing the wave function to delocalize and overlap with the wave function in the adjacent wells. Thus, using standard QWIP designs and pushing them toward the longer wavelengths, will require thicker barriers than their mid infrared counterparts to keep the sequential tunneling to the same values.

In addition, the rather small decay constants (less than 20Å) demonstrate that increasing the barrier width is an effective means of reducing the sequential tunneling contribution to the dark current.

The sequential tunneling contribution to the dark current will decay by many orders of magnitudes when

the barrier width is increased to 160Å^[6]. Given a QWIP with a particular detection wavelength and measured dark current, this empirical relationship could be used to deduce the required barrier width to design the dark current to meet a specific requirement.

The data in Table 1 shows that for every 9.5Å increase in barrier width of a particular 9.7µm QWIPs design, the phonon sequential tunneling contribution will be reduced by a factor of e⁻¹. To reduce this contribution by a factor of 10⁻³ implies that the barrier width must increase by an amount ΔL_b = 66Å.

Reducing sequential tunneling with thermal excitation and thermionic emission: The constructed model is defined for evaluating the effects of thermionic emission and thermally-assisted tunneling on the dark current. Calculated results using this model agree with experiments in a QWIP in which the dominant dark current mechanisms are due to thermionic emission and thermally-assisted tunneling which has been used until recently. The dark current of a QWIP is given by^[4]:

$$I_d = \frac{em_w^* A_{DET}}{\pi \hbar l_p^2} \cdot \frac{\mu F}{\sqrt{1 + (\mu F / v_s)^2}} \int_{\epsilon_1}^{\infty} f(\epsilon) T(\epsilon, F) d\epsilon \quad (3)$$

where m_w^{*} is the electron effective mass in the QW, A is the device area, l_p = (l_w + l_b) is the QWIP period length, μ is the electron mobility, F = V_b / Nl_p is the electric field inside the QWIP, v_s is the electron saturation velocity, f(ε) is the Fermi-Dirac distribution function and T(ε, F) is the bias-dependent tunneling current transmission coefficient for a single barrier defined by:

$$T(\epsilon, F) = \begin{cases} 1, & \epsilon \in I \\ \exp\left(-\frac{4}{3e\hbar F} (2m_b^*)^{1/2} (\epsilon_b - \epsilon - eFl_w)^{3/2}\right), & \epsilon \in II \\ \exp\left\{ \begin{aligned} &-\frac{4}{3e\hbar F} (2m_b^*)^{1/2} \\ &\times \left\{ \begin{aligned} &(\epsilon_b - \epsilon - eFl_w)^{3/2} \\ &-(\epsilon_b - \epsilon - eF(l_w + l_b))^{3/2} \end{aligned} \right\} \end{aligned} \right\}, & \epsilon \in III \end{cases} \quad (4)$$

and the triple energy regions are

$$\begin{cases} I : \epsilon > \epsilon_b - eFl_w \\ II : \epsilon_b - eF(l_w + l_b) \leq \epsilon \leq \epsilon_b - eFl_w \\ III : \epsilon_1 \leq \epsilon \leq \epsilon_b - eF(l_w + l_b) \end{cases}$$

where l_w is the well width, l_b is the barrier width, m_b^{*} is the electron effective mass in the barrier and ε_b is the barrier height.

In Eq. 3, the first parameter which effectively reduces the dark current is the detector dimension. The dark current characteristics as a function of the bias voltage for A_{DET} = (250 µm)² and A_{DET} = (200 µm)² are depicted in Fig. 3. As shown, reducing the detection area decreases the dark current. By increasing the bias voltage, the dark current is increased and then saturated.

The second parameter is Al density which reduces the dark current at low level bias voltage. It also influences the effective mass of the barrier m_b^{*} and the barrier height ε_b^[8-9]. Figure 4 shows the dark current characteristics for x = 0.25 and x = 0.164. The increase of x in a fixed bias voltage reduces the dark current (V_b < 2V), whereas the same change in x does not have any remarkable effect at higher voltages. Equality of the dark current in both curves of the Fig. 4 at high level bias voltages is due to stronger bias electric field which in turn increases the tunneling probability of the upper triangular edge of the barrier in thermal excitation via increase of the barriers number.

As illustrated in Fig. 5, increasing the number of periods decreases the dark current because of decreasing the average electric field through the device. Also, increasing the number of periods reduces the detector responsivity^[10]; hence it should be optimally designed through judicious choice. Fig. 6 shows the behavior of the dark current density as a function of bias voltage for different height of barrier near the emitter which decreases with increasing the height^[5].

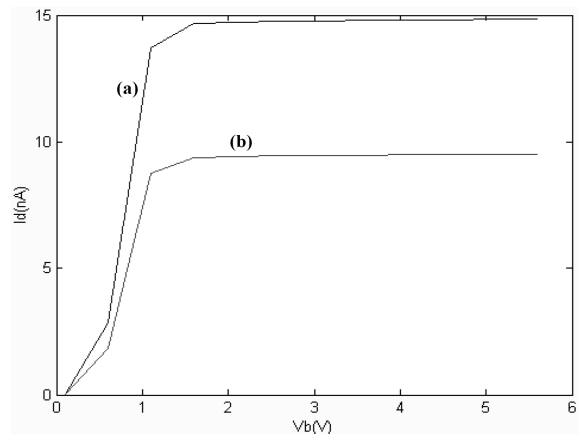


Fig. 3: The dark current as a function of bias voltage for a QWIP at 77°K with N = 50, L_b = 500Å, L_w = 50Å, ε₁ = 20meV, ε_f = 43mV, ε_b = 137meV, x = 0.1640. (a) A_{DET} = (250µm)² and (b) A_{DET} = (200µm)²

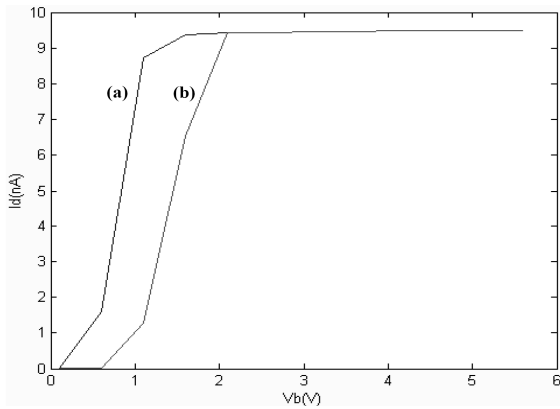


Fig. 4: The dark current as a function of bias voltage for a QWIP at 77°K with $N = 50$, $L_b = 500\text{\AA}$, $L_w = 50\text{\AA}$, $\epsilon_1 = 20\text{meV}$, $\epsilon_f = 43\text{mV}$, $\epsilon_b = 137\text{meV}$, $A_{\text{DET}} = (200\mu\text{m})^2$ (a) $x = 0.1640$ and (b) $x = 0.25$

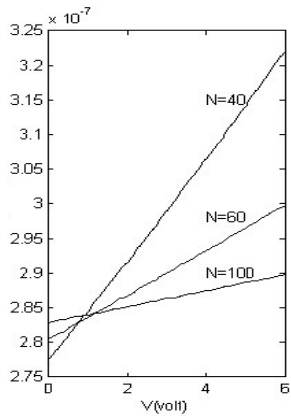


Fig. 5: The dark current as a function of bias voltage for different number of periods

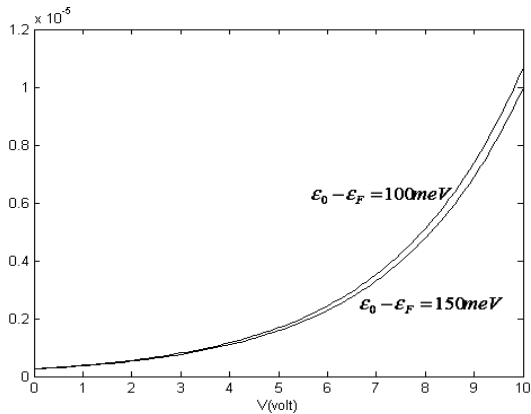


Fig. 6: The dark current density as a function of bias voltage for different height of barrier

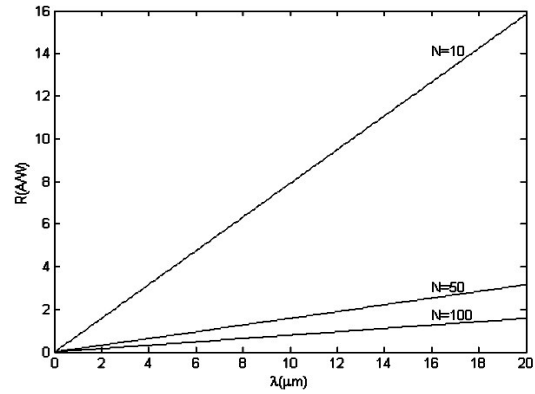


Fig. 7: Responsivity as a function of wavelength for different numbers of period

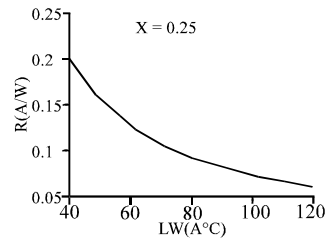


Fig. 8: Responsivity as a function of well width

Responsivity and detectivity: The responsivity of a QWIP is commonly used figure-of-merit for detector performance and is given by:

$$R = \frac{e\eta}{h\nu} \lambda \frac{1 - P_c}{P_c} \cdot \frac{1}{N} \tag{5}$$

where η is the quantum efficiency of a single well, N is the period number and P_c is the quantum well capture probability^[10]. The responsivity can be expressed as a function of well width:

$$R = \frac{e\eta}{hcN} \lambda \frac{\exp\left(\frac{-L_w}{L_c}\right)}{1 - \exp\left(\frac{-L_w}{L_c\lambda}\right)} \tag{6}$$

where L_c is a decay constant defining the rate of increase of the capture probability P_c with well width L_w .

Figure 7 shows the responsivity (R) as a function of detection wavelength λ for fixed capture probabilities P_c and varying number of periods. It can be seen that there is a direct proportionality between R and λ . Also the responsivity increases superlinearly with detection wavelength. Figure 8 shows the results

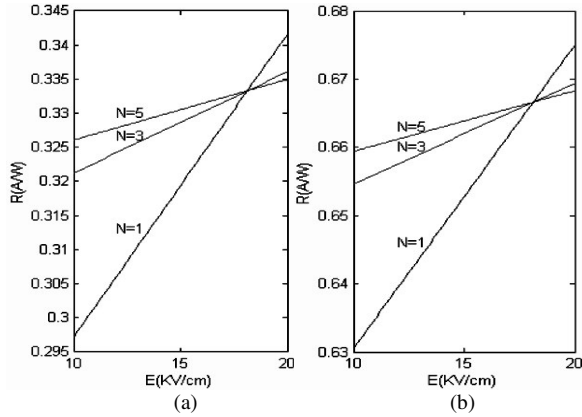


Fig. 9: Responsivity as a function of the average electrical field (a) $\Sigma_d = 0.5 \times 10^{12}/\text{cm}^2$ and (b) $\Sigma_d = 1 \times 10^{12}/\text{cm}^2$

of calculations of the responsivity versus the quantum well width.

The responsivity as a function of the average electric field for different donor sheet densities is shown in Fig. 9. The responsivity slowly decreases with the decrease of average electric field. However, it is valid until the electric field is able to extract the electrons into the collector. If the electric field at the collector tends to zero, the extraction of the electrons from the QW structure decreases and the potential distribution and the electric field at the emitter become insensitive to the electron photo-excitation. It leads to a drastic drop in the responsivity^[5].

A general formula for the QWIP frequency-dependent responsivity is given by:

$$R_\omega = R_0^* \frac{2}{i\omega\tau(N+1)} \frac{e^{i\omega\tau} - 1}{(1 - Be^{i\omega\tau})^2} \times \frac{1}{[B^{N+1}e^{i\omega\tau(N+1)} - B(N+1)e^{i\omega\tau} + N]} \quad (7)$$

where B is the capture parameter of the electron passed the QW ($0 < B < 1$), τ is the electron transit time, $R_0^* = e\sigma \sum_0 / 2h\Omega$, \sum_k is the electron sheet concentration in the k^{th} QW (in the bound state), σ is the photo-excitation cross-section and $h\Omega$ is the photon energy^[11].

Using the noise model^[12], we have calculated the noise gain of the device and the peak detectivity. The detectivity can be expressed as

$$D_\lambda^* = R \sqrt{\frac{A_{DET} \Delta f}{4eI_d g}} \quad (8)$$

where R is the responsivity, A_{DET} is the device area, Δf is the bandwidth, e is the electron charge, I_d is the dark

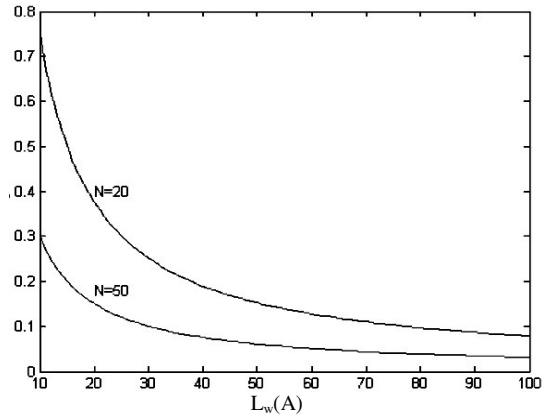


Fig. 10: Gain as a function of width length

current and g is the noise gain which can be expressed as:

$$g(V) = \frac{I_d R_0}{\frac{kT}{c} N^2 \exp\left(\frac{\Delta E}{kT}\right)} \quad (9)$$

where R_0 is the dynamic resistance at zero bias, N is the period number, K is the Boltzmann constant and ΔE is the barrier lowering given by:

$$\Delta E = e \sqrt{\frac{eV_b}{4l_p \pi \epsilon_0 \epsilon_r}} \quad (10)$$

where V_b is the bias voltage across one period and l_p is one period length^[12-13].

The photocurrent gain is viewed in terms of a quantum well capture probability (P_c) and is derived from^[14],

$$g = \frac{1 - P_c}{P_c(N+1)} + \frac{1 - (1 - P_c)^{N+1}}{P_c(N+1)^2 [1 - (1 - P_c)^{N+1}]} \quad (11)$$

Figure 10 illustrates the gain as a function of well width for different number of periods.

THE DESIGN OF OPTIMAL PHOTODETECTOR

Following the above mentioned remarks, the design objective is the minimization of the dark current at 77°K.

Determination of quantum well dimensions

Well depth: The depth of the quantum well (V_0) is determined by considering the energy of the absorbed photons.

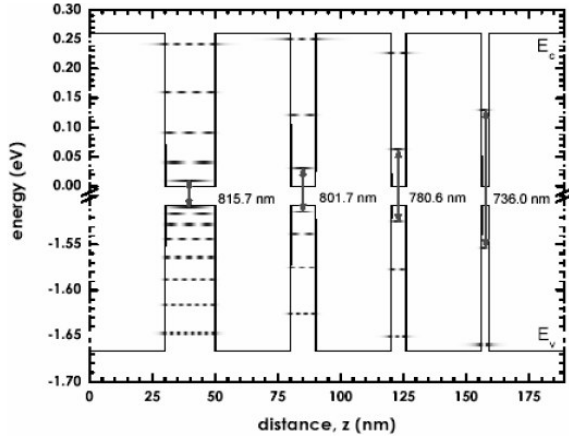


Fig. 11: Energy band diagram of the GaAs/AlGaAs QWIP structure^[15]

$$V_0 \approx \epsilon_p = \frac{hc}{\lambda} \quad (12)$$

where λ is the wavelength of responsivity peak and ϵ_p is the energy of absorbed photons, then

$$V_0 \leq \epsilon_p + \epsilon_1 \quad (13)$$

where ϵ_1 is the energy of the first confined level of potential well. On the other hand,

$$V_0 \leq 139meV + \epsilon_1 \quad (14)$$

Well thickness: The results of Workman simulation revealed that the number of sub-bands increases with well widening (Fig. 11)^[15]. However, the quantization condition and the energy levels of wells^[9] are respectively given by:

$$l_w \ll \frac{\pi\hbar}{\sqrt{2kTm_w^*}} \quad (15)$$

$$\epsilon = \frac{(\hbar\pi l)^2}{2m_w^* l_w^2} \quad (16)$$

Then for $\epsilon_p = 139meV$ and $m_w^* = 0.067m_0$, $l_w = 50\text{\AA}$ is obtained.

Barrier width: To reduce the effects of tunneling on the dark current, the barrier width should be increased as much as possible. A suitable criterion for barrier width is $l_b = 10l_w$.

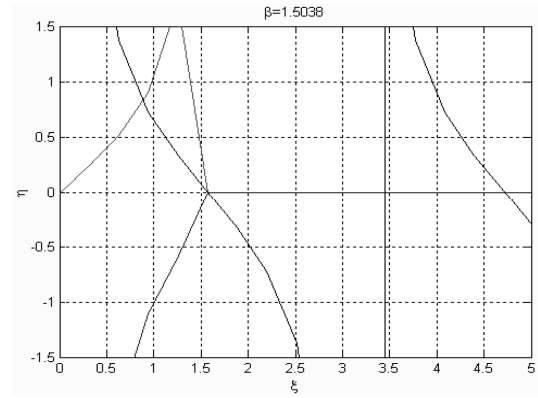


Fig. 12: Schematic presentation of η_{even} , η_{odd} and $\cot(\xi)$ for finding the base energy of detector

Determination of Al density and base sub-band energy: Increasing Al density will decrease the dark current. To calculate Al density (x), we use the following relation suitable for $\text{Al}_x\text{Ga}_{1-x}\text{As}$ structure^[9]:

$$x = \frac{V_0 (meV)}{835.5} \quad (17)$$

Substitution of $V_0 = 150meV$, leads to $x = 0.18$. To modify the dark current and to optimize the well depth, we assume x to be 0.25 and then, $V_0 = 209meV$. In addition the effective mass of the carriers in the barriers is given by $m_b^* = (0.067+0.083x)m_0$, Hence, $m_b^* = 0.0878m_0$.

In addition Eq. 7 leads to $\epsilon_1 > 70meV$ and β is defined as^[16],

$$\beta = \frac{l_w \sqrt{2m_w^* V_0}}{2\hbar} = 1.5038. \quad (18)$$

As shown in Fig. 12 (η as a function of ξ for $\beta = 1.5038$), the well can only have an even base state for $\xi = 0.9$. Hence, the wave number becomes:

$$k_w^{\text{even}} = \frac{2\xi}{l_w} = 3.6 \times 10^{-2} (1/\text{\AA}) \quad (19)$$

and the energy associated to even base state is:

$$\epsilon_1 = \frac{(k_w^{\text{even}} \hbar)^2}{2m_w^*} = 75meV \quad (20)$$

In Fig. 13, potential well designed for optimal QWIP, the base energy level and its eigen function are

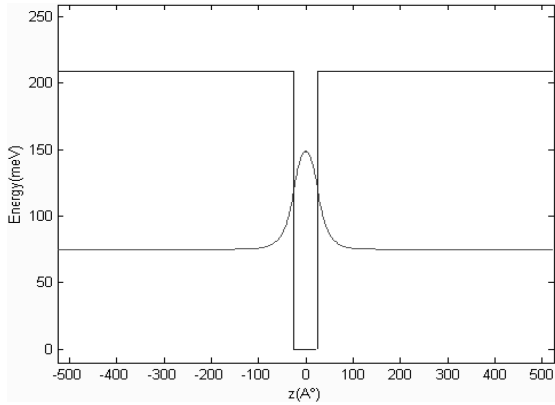


Fig. 13: Schematic representation of the potential well designed for optimal QWIP, base energy level and eigenfunction

shown. In addition to performing precise design steps for detection wavelength, the well depth is also enhanced. Increasing the well depth increases the trapping of thermionic emission carriers and hence, the dark current is more reduced. In other words, we have designed an energy filter which prevents transfer of the dark current carriers. These carriers generally have less energy than photoelectrons.

Determination of the optimum period number: Increasing the number of periods reduces both responsivity and the dark current. On the other hand, detection coefficient increases with increasing the number of periods. Considering the discussed factors and assuming $N = 50$, the dark current is constrained to 10nA.

RESULTS AND DISCUSSION

The designed parameters of the detector are presented in Table 2. Also the achieved performance characteristics of the optimized device are presented in Table 3 that reveals the excellent detectivity and low dark current of designed photodetector.

Figure 14 shows the dark current as a function of the bias voltage in QWIP. The value of dark current is approximately 11nA for voltages more than 1V in temperature 77°K. The responsivity value was calculated assuming a constant quantum efficiency of 10% and a quantum well captures probability of 6% which is typical of many devices. In addition, as shown in Fig. 15, the device bandwidth is 400GHz that can be achieved from Eq. 7.

Table 2: The main characteristics of designed photodetector with ultra low dark current

Parameter	value
T	77°K
V_{barrier}	209meV
ϵ_1	75meV
R_0	10^7
m_b	0.0836 m_0
m_w	0.067 m_0
L_b	500Å
L_w	50Å
n	10^{18}cm^{-3}
η	0.1
N	50
A_{DET}	$1.6 \times 10^{-3} \text{cm}^2$
x	0.25

Table 3: The achieved performance data of designed photodetector

Parameter	value
R	166mA/W
I_d	11nA
D^*	$1.42 \times 10^{12} \text{cm} (\text{Hz})^{1/2}/\text{W}$
Δf	400GHz

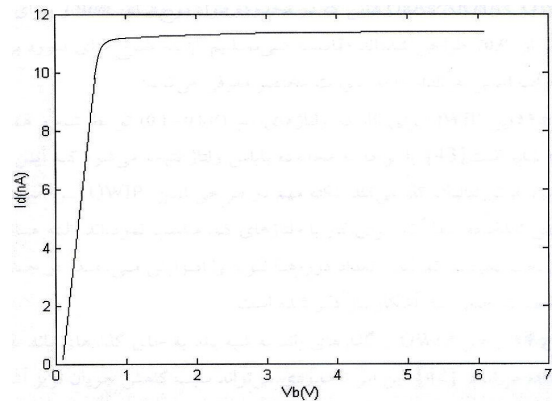


Fig. 14: The dark current as a function of bias voltage in optimal QWIP

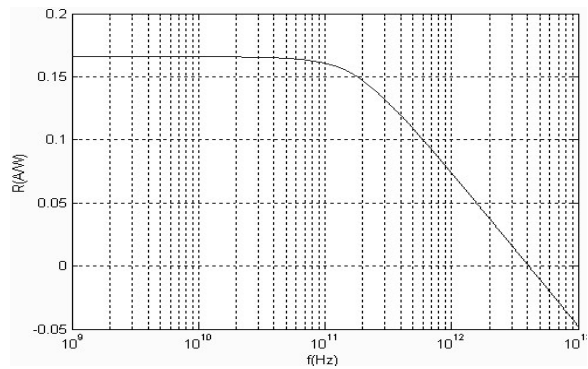


Fig. 15: Frequency response of designed QWIP

CONCLUSION

The QWIP performance has been improved by an order of magnitude in detectivity and dark current. Investigation of different contributors to the dark current in GaAs/AlGaAs QWIPs proved that optimal determination of physical dimensions of the photodetector, the periodic length of the structure, Al density and the number of periods reduce the dark current by an order of magnitude 11 nA and thereby significantly increase the detectivity about $10^{12}\text{cm}(\text{Hz})^{1/2}/\text{W}$.

REFERENCES

1. Gunapala, S.D., J.S. Park, G. Sarusi, L. True_Lon, J.K. Liu and P.D. Maker, 1997. 15 μm 128 \times 128 GaAs/Al_xGa_{1-x}As quantum well infrared photodetector focal plane array camera: IEEE Trans. Electron Devices, 44 (1): 45-50.
2. Moon, J., S.S. Li and J.H. Lee, 2003. A high performance quantum well infrared photodetector using superlattice-coupled quantum wells for long wavelength infrared detection: Infrared Phys. Technol., 44 (4): 229-234.
3. Ettech, N.E.L and P. Harrison, 2001. Carrier scattering approach to the origins of dark current in mid-and far infrared (Terahertz) quantum well intersub-band photodetectors (QWIPs): IEEE J. Quantum Electronics, 37 (5): 672 - 675.
4. Levine, B.F., C.G. Bethea, G. Hansian, V.O. Shen, E. Pelve, R.R. Abbott and S.G. Hesieh, 1990. High sensitivity low dark current 10 μm GaAs quantum well infrared photodetectors: Appl. Phys. Lett., 56 (9): 851-853.
5. Ryzhi, V., 1997. Theory of quantum well IR photoconductors with tunneling electron injection: IEE Optoelectron., 44 (5): 343-349.
6. Gunapala, S.D., G. Surasi, J. Park, T. Lin and B.F. Levine, 1994. Infrared detectors reach new length: Phys. World, 7: 35.
7. Liu, H.C., A.G. Steele, M. Buchanan and Z.R. Wasilewski, 1993. Dark current in quantum well infrared photodetector: J. Appl. Phys., 73: 2029.
8. Shur, M., 1999. Physics of semiconductor devices. Prentice-Hall International, Inc.
9. Petter, S. and J.R. Zory, 1993. Quantum Well Lasers. Academic Press, Inc.
10. Gadir, M.A. and P. Harison, 2002. Responsivity of quantum well infrared photodetectors (QWIPs) at Terahertz wavelength: Appl. Phys. Lett., 91 (9): 5820-5825.
11. Ryzhii, V., I. Khmyrova and M. Ryzhii, 1998. Impact of transit time and capture effects on high frequency performance of multiple quantum-well infrared photodetectors: J. IEEE, Electron Devices., 45 (1): 293-298.
12. Jians, X., S.S. Li and M.Z. Tidrow, 1999. Investigation of a multistack voltage tunable for color quantum well infrared photodetectors for mid and long wavelength infrared detection: IEEE Trans. Quantum Electronics, 35 (11): 1685-1693.
13. Gunapala, S.D., S.V. Bandara, A. Singh, J.K. Liu and B. Rafol, 2000. 640 \times 486 long wavelength two color GaAs/Al_xGa_{1-x}As quantum well infrared photodetector (QWIP) focal plane array camera: IEEE Trans. Electron Devices, 47 (5): 963-971.
14. Ershov, M. and H.C. Liu, 1999. Low-frequency noise gain and photocurrent gain in quantum well infrared photodetectors: J. Appl. Phys., 86 (11): 6580-6585.
15. Workman, C.L., 2002. Intersub-band transitions in strained InGaAs quantum wells for multi-color infrared detector applications: PhD Thesis, University of Arkansas.
16. Loher, J.P., 1998. Physics of strained quantum well lasers. Kluwer Academic Publisher.